Inferring the maximum and minimum mass of merging neutron stars with gravitational waves

Katerina Chatziioannou[1] and Will M. Farr[1, 2]

[1]*Center for Computational Astrophysics, Flatiron Institute, 162 5th Ave, New York, NY 10010, United States*
[2]*Department of Physics and Astronomy, Stony Brook University, Stony Brook NY 11794, United States*
(Dated: May 4, 2020)

We show that the maximum and the minimum mass of merging neutron stars can be estimated with upcoming gravitational wave observations. We simulate populations of binary neutron star signals and model their mass distribution including upper and lower cutoffs. The lower(upper) limit can be measured to $\sim 0.2(0.1)\mathrm{M}_\odot$ with 50 detections if the mass distribution supports neutron stars with masses close to the cutoffs. The upper mass limit informs about the high density properties of the neutron star equation of state, while the lower limit signals the divide between neutron stars and white dwarfs.

INTRODUCTION

Despite being first detected more than 50 years ago, the properties of neutron stars (NSs) such as their possible masses and sizes are still uncertain [1, 2]. Coalescences of NSs, now observable with gravitational waves (GWs) [3, 4] by LIGO [5] and Virgo [6], can offer information about both, through measurement of the binary component masses and tidal interactions between the two stars as they are about to merge [7]. The masses of NSs offer information both about the astrophysics of compact objects, and about the dense matter NSs are made of.

Stable nonrotating NSs have a maximum possible gravitational mass $M_{\max}$ beyond which internal pressure cannot support them against gravitational collapse towards black holes (BHs). The maximum mass is a function of the unknown equation of state (EoS) of NSs that governs the properties and composition of their interiors though rotation can offer additional support, increasing $M_{\max}$ by about 20% [8]. The detection of heavy pulsars through radio surveys has placed a robust lower limit of $M_{\max} \gtrsim 2\mathrm{M}_\odot$ [9, 10], suggesting that the high-density EoS is stiff enough to support them against collapse. This poses a challenge in particular for models predicting phase transitions inside NSs that result in a softening of the EoS and lower the maximum mass possible [11]. The mass distribution of galactic NSs offers tentative evidence for an upper cutoff at $2.0-2.6\mathrm{M}_\odot$ [12, 13], while assuming that merging NSs follow the galactic double NS distribution and produce the observed gamma ray bursts led to $M_{\max} \lesssim 2.0 - 2.2\mathrm{M}_\odot$ before the detection of GWs [14].

Current GW observations are consistent with NSs with masses below $2\mathrm{M}_\odot$, but they have been used to study the maximum NS mass by considering the merger outcome [15–17] or EoS modeling. Interpretating the electromagnetic counterpart to GW170817 as supporting the formation of a hypermassive NS remnant that eventually collapsed to a BH and assumptions about the post-merger evolution of the system suggest $M_{\max} \lesssim 2.3\mathrm{M}_\odot$ [18–23]. In parallel, tidal interactions in GW170817 offer constraints on the low-density EoS. Extrapolating to high-densities using a model for the EoS based on a gaussian process conditioned on existing nuclear models yields $M_{\max} \lesssim 2.4\mathrm{M}_\odot$ [24, 25].

It is unknown whether stellar evolution can produce NSs up to the maximum mass allowed by nuclear physics and BHs down to the most massive NSs. X-ray observations provide tentative evidence for a mass gap between the heaviest NS and the lightest BH, though its existence is under debate [26, 27]. Recent observations suggest the existence of objects in the mass gap, though it is unknown whether they are NSs or BHs [28]. The minimum mass of astrophysical NSs $M_{\min}$ is expected to be entirely driven by their formation mechanism and might inform the divide between NSs and the next most-compact object, white dwarfs (WDs).

Observational campaigns and improved detector sensitivity are expected to yield dozens of binary NS (BNS) detections through GWs in the coming years [29]. We examine whether these observations can be used to extract the mass distribution of coalescing NSs and in particular the maximum and minimum mass. We find that $M_{\max}$ can me measured to within $\sim 0.2M_\odot$ and $M_{\min}$ to within $\sim 0.1M_\odot$ at the 90% level with 50 observations if the mass distribution has support for heavy and light NSs. The $M_{\max}$ constraint can reduce the uncertainty about the pressure at 4.5 times saturation density by $\sim 20\%$. However, if binary formation mechanisms lead to a mass distribution that smoothly tails off on the high or low end, the measurement uncertainties for $M_{\max}$ and $M_{\min}$ correspondingly increase. Our estimates are conservative as we impose no restrictions on the potential NS spins, which leads to larger mass uncertainties compared to assuming that merging NSs are slowly spinning, per galactic observations [30]. Our mass estimates are solely based on the inferred masses and are not subject to systematics related to tidal inference, EoS modeling, or the interpretation of a possible electromagnetic counterpart.

A POPULATION OF BNS SIGNALS

Similar to BH binaries, the mass distribution of NSs in binaries depends on the formation mechanism. The minimum possible NS mass is related to the transition between WDs and NSs, while the absolute maximum is driven by the unknown EoS. However, it is unclear if binary evolution can result in systems with components close to the extremes, either for BHs or NSs. Given these uncertainties and evidence suggesting that merging NSs have a different mass distribution than the observed galactic double NSs [4], we consider three mass distributions and simulate populations of potentially observable BNSs: (i) the masses m_1, m_2 are uniformly distributed in $[M_{\min} = 1, M_{\max} = \{2.0, 2.2\}]M_\odot$ with $m_1 > m_2$ ("Uniform"), (ii) the primary mass m_1 is uniformly distributed in $[M_{\min} = 1, M_{\max} = \{2.0, 2.2\}]M_\odot$ while the mass ratio $q \equiv m_2/m_1$ favors equal masses as suggested by [31]; we use a q^3 distribution ("UniformQ"), and (iii) the primary mass m_1 is distributed according to a bimodal distribution as suggested in [12, 13] based on galactic NSs with $M_{\min} = 1M_\odot$, $M_{\max} = \{2.0, 2.2\}M_\odot$ while the mass ratio goes as q^3. We repeat the analysis of [13] including the recent observation from [10] and select a fair draw from the mass distribution posterior ("Bimodal")[1]. We do not consider a single gaussian distribution [32], as GW190425 might suggest that merging BNSs do not follow it [4]. In all cases, the sharp upper cutoff in the mass distribution is related to the NS EoS, however the "Bimodal" distribution exemplifies a situation where the binary formation mechanism reduces the rate of heavy NSs in binaries independently of the EoS.

Given the parameters of a simulated BNS, we approximate measurement uncertainty with the methods described in the supplemental material. Rather than assuming a gaussian likelihood in the parameters of interest as is common, we utilize the fact that information about the binary parameters comes from modeling the phase evolution of the GW signal [33]. We instead assume gaussian likelihoods in the coefficients of the Taylor expansion of the GW phase around small velocities. This method is able to capture the effect of the mass-spin degeneracy [34], resulting in asymmetric likelihoods for the mass ratio and the effective spin of the binary. In order to be conservative, we do not impose that the spin of the NSs is small, which results in a larger uncertainty on the binary mass ratio, see for example the high-spin and low-spin inference for GW170817 in [35].

We model the simulated BNS populations with the hierarchical formalism of [36] while simultaneously fitting for the true masses of each observed event [37]. We con-

sider two mass models for the primary mass and the binary mass ratio: (i) a power law for both -with which we fit the "Uniform" and "UniformQ" populations-

$$P(m_1, q|\alpha, \beta) \sim m_1^{-\alpha} q^\beta, \qquad (1)$$

and (ii) a two-gaussian distribution for the primary mass with a power law for the mass ratio -with which we fit the "Bimodal" population-

$$P(m_1, q|A, \mu_1, \sigma_1, \mu_2, \sigma_2) \sim$$
$$[A\kappa_1 \mathcal{N}(m_1; \mu_1, \sigma_1) + (1 - A)\kappa_2 \mathcal{N}(m_1; \mu_2, \sigma_2)] q^\beta. \quad (2)$$

where the $\kappa_{1,2}$ are chosen so each Gaussian integrates to 1 over $M_{\min} < m_1 < M_{\max}$, which means A is the fraction of NSs associated to the first Gaussian.

GW observations are subject to a strong selection bias towards more massive events that emit stronger signals. For low-mass binaries the selection effect can be analytically approximated as the probability that an event is observed is proportional to $\mathcal{M}^{5/2}$. We take this selection effect into account both in our simulated population (where the observed population contains more heavy systems than the intrinsic population) and in the hierarchical inference in order to avoid biases [38, 39].

Figure 1 shows the "UniformQ" (top) and "Bimodal" (bottom) primary mass distributions, inferred from a simulated population of 50 observations with realistic measurement uncertainties. Both populations have a sharp upper limit (pink histograms). The lack of observations with masses above that value -especially since they are favored by selection effects- results in a similarly sharp cutoff in the inferred distribution (green shaded regions). The minimum mass does not result in a sharp cutoff of the m_1 distribution as $m_2 < m_1$, but in a gradual decline. This decline together with the inferred mass ratio distribution result in a measurement of $M_{\min}$.

RESULTS

The chirp mass $\mathcal{M}$ is the best measured intrinsic parameter for all binaries observed to date [40] and largely drives mass inference, especially for low mass systems. Its inferred value provides a sharp cutoff for both the maximum and the minimum mass possible for the binary components of $2^{1/5}\mathcal{M}$. For example, from the inferred chirp mass alone we know that GW170817 contains an object with mass $\lesssim 1.36M_\odot$ [35], while GW190425 has an object with a mass $\gtrsim 1.65M_\odot$ [4], providing some first crude bounds on $M_{\min}$ and $M_{\max}$ from GWs. The same applies to our simulated populations, where we expect sharp upper and lower limits on $M_{\min}$ and $M_{\max}$ based on the smallest and largest observed $\mathcal{M}$ respectively.

Figure 2 shows the expected measurement uncertainty for $M_{\min}$ and $M_{\max}$ as a function of the number of observed signals N for different mass distributions averaged

---

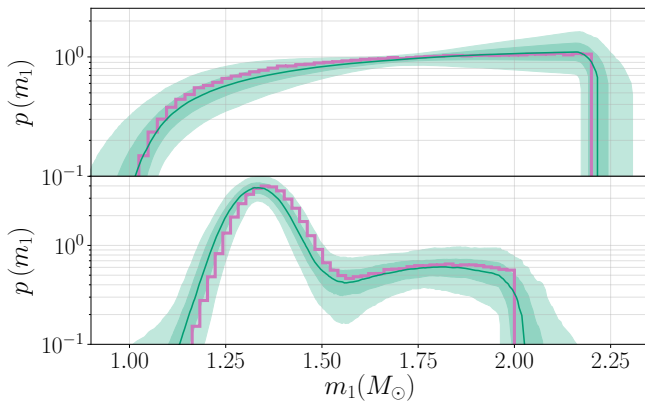[1] Model and samples are available in https://github.com/farr/AlsingNSMassReplication.

FIG. 1. Primary mass distribution inferred from 50 simulated BNS detections. The pink histogram is the true distribution. The green line and shaded regions are the median, 50%, and 90% credible intervals of the inferred distribution respectively. Top: uniform distribution. Bottom: bimodal distribution.

over population realizations. Shaded regions correspond to highest probability density intervals, though the $M_{\min}$ and $M_{\max}$ posteriors are fairly asymmetric due to the effect described above. In all cases we find that we can extract the correct values, as expected for inference where the model matches the intrinsic distribution of sources.

We find that if NS masses are uniformly distributed (green and orange) $30-50$ signals, potentially detectable during the fourth observing run circa 2022 [29], can lead to an estimate of $M_{\min}$ to within $\sim 0.2 M_\odot$ and $M_{\max}$ within $\sim 0.1 M_\odot$ at the 90% level. Further detector improvements and new observatories can potentially lead to the detection of $100-200$ systems, though estimates are uncertain [29]. With 200 detections we can extract $M_{\min}$ to within $\sim 0.1 M_\odot$ and $M_{\max}$ within $\sim 0.05 M_\odot$ at the 90% level using GW mass inference alone.

If the NSs observed by GW detectors follow a bimodal distribution instead, then we expect fewer NSs close to the maximum and minimum, and all constraints are correspondingly weaker. This could, for example, be the case if binary formation disfavors systems containing the heaviest/lightest possible NSs; even in this case, though, any sharp upper cutoff in the mass distribution is the result of the nuclear EoS. Our assumed bimodal mass distribution has $(\mu_1, \sigma_1, \mu_2, \sigma_2) = (1.35, 0.07, 1.85, 0.35) M_\odot$ and $A = 0.63$, implying $0.12N(0.05N)$ systems with $m_1 > 2.0(2.2) M_\odot$; these parameters are a "fair draw" from the posterior over NS mass distributions fitted to galactic pulsars [13]. Our mass model "learns" the maximum (minimum) NS mass from the absence of observed events above (below) the cutoff mass. Such an absence can only be inferred confidently when the corresponding smooth mass distribution without the cutoff would have produced several events above (below) the cutoff. If the smooth distribution predicts 5 "missing systems" above (below) the cutoff, the probability of observing none is

smaller than 1%, and the existence of a cutoff can be confidently inferred; for the bimodal mass distribution, $N \sim 50(100)$ detections would yield ~ 5 detections above $M_{\max} = 2.0(2.2) M_\odot$. We therefore expect that 50–100 detections from the bimodal mass distribution are required to confidently identify the cutoff mass scale. This expectation is confirmed by Fig. 2 where we plot both the 70% (dark) and 90% (light shading) credible interval on the cutoff masses. The posteriors for $M_{\max}$ and $M_{\min}$ are highly asymmetric because the cutoff must always be larger/smaller than the heaviest/lightest observation, but generally less constrained in the opposite direction.

The above estimates assume no a priori restrictions on the NS spins; instead assuming that merging NSs have low spins would result in tighter inference of all parameters by mitigating the spin -mass ratio correlation [35].
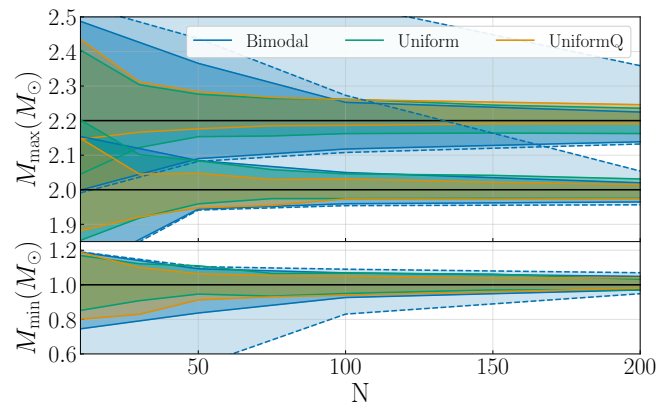

FIG. 2. Highest probability credible intervals on the maximum (top) and the minimum mass (bottom) as a function of the number of detections, averaged over 20 populations. Solid horizontal lines denote the true value. For the "Uniform" and "UniformQ" distributions we show 90% intervals. For the "Bimodal" distribution we show 70% (dark) and 90% (light shading) intervals. The intervals are asymmetric because the maximum and minimum masses must enclose all observed events, but are typically less constrained away from the observed masses.

DISCUSSION

A robust determination of the maximum and minimum NS mass can have implications for our understanding of the high-density EoS of NSs. The ever increasing lower bound on the maximum mass driven from pulsar observations has been used to rule out the softest EoS models, leading to the current picture of EoSs predicting almost constant radii for NSs in the range $1-1.8 M_\odot$ [1]. An upper limit on the maximum mass should lead to a complementary constraint on the stiffness of the EoSs.

Figure 3 sketches the effect of potential maximum mass constraints on EoS inference for GW170817 [41–43]. The

blue band corresponds to current constraints that already assume that the maximum mass is above $1.97M_\odot$ [9]. Incorporating new M_{max} constraints would preferably make use of the full inferred distribution [44] while avoiding biases caused by mishandled Occam penalties [45]. However, we can make a quick estimate of the effect of M_{max} on EoS inference by imposing an upper and a lower limit on M_{max} corresponding to its 90% interval after the detection of ~ 50 BNS signals with the "UniformQ" distribution. The green shaded band is the result of an even more stringent lower limit on M_{max} and it rules out some of the soft parameter space at pressures around 4-5 times the nuclear saturation density. Adding an upper limit on M_{max} leads to the pink shaded region which additionally constrains the stiff part of the EoS at similar densities.

Overall, a $\sim 6\%$ constraint on M_{max} leads to a constraint of the pressure at 4.5 times the saturation density of $\sim 20\%$, possible with ~ 50 detections. Such constraints on the high-density EoS might only be achievable through measurements of M_{max} in the near future. Tidal measurements of binaries with masses close to maximum are intrinsically challenging as tidal interactions are weaker for more massive NSs [7, 46, 47]. Further GW probes of high densities such as post merger emission from a hyper massive remnant are expected to be detected on longer timescales than the first 50 BNS signals [48]. Finally, an accurate measurement of M_{max} can be compared to tidal inference from the BNS inspiral which probes the low-density EoS to potentially probe signatures of a phase transition in the EoS [11, 15, 49, 50].
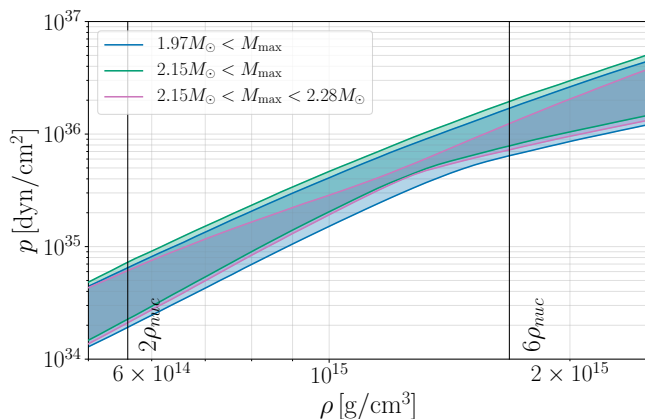

FIG. 3. Effect of a maximum mass constraint on EoS inference. We plot 90% credible intervals for the NS pressure as a function of the density for GW170817 under different potential maximum mass knowledge. As expected, the maximum NS mass offers information about the high-density EoS, around $4-5$ times the nuclear saturation density.

On the astrophysical side, a determination of M_{min} could inform the boundary between WDs and NSs. Ground based GW detectors are deaf to signals from binaries containing WDs; the orbital separation of a binary emitting at 10Hz -a common lower boundary on the LIGO bandwidth- is ~ 600km for a total mass of $2M_\odot$. Any binary containing WDs would merge below 10Hz and so any inspiral signal seen in LIGO must contain objects more compact than WDs. Determination of M_{min} could aid the classification of low-mass binary components and inform about their formation [51].

Besides WDs, BHs that form through stellar evolution are expected to be heavier than NSs and not lead to a contamination of the BNS population. However, exotic possibilities such as primordial BHs or merger products could occupy any mass range, even below $1M_\odot$. Searches for subsolar mass binaries through GWs place upper limits on their abundance [52–54] however these are less stringent than the upper limit of the inferred BNS rate [4] due to the decreased detector sensitivity to low mass signals. Such BHs could be differentiated from NSs by the fact that the latter are expected to be subjected to strong tidal effects, while the former do not [55]. On the high mass side, the existence of BHs with masses comparable to the most massive NSs would alter the mass distribution of low-mass objects. If low-mass BHs are, as expected, less abundant than NS of similar mass, then the mass distribution would no longer terminate at M_{max}, but it would exhibit a sharp drop. This sharp drop can be detected with methods similar to the ones applied here. If, on the other hand, BHs outnumber NSs in the $2-3M_\odot$ range, then telling them apart will be very challenging, requiring electromagnetic observations [56] or next generation detectors that could constrain the tidal signature of $\sim 2M_\odot$ compact objects [57].

A sharp feature in the NS mass distribution could in principle break the degeneracy between distance and redshift in GW observations and lead to constraints on the Hubble constant H_0 [58]; a similar approach has been proposed for BHs [59]. However, for a typical distance uncertainty of 50% [60] and an uncertainty of $0.1M_\odot$ in the cutoff mass, local ($z \lesssim 0.1$) signals will not provide sufficient accuracy in the redshift measurement to permit measurement of H_0 comparable with competing constraints [61]. With third-generation GW detectors [62, 63] the reach for neutron star systems extends to sufficiently high redshift that a $0.1M_\odot$ mass uncertainty would be sufficient to determine the redshift-distance relation at the sub-percent level [64], but by the time such detectors are operating other GW methods [61] will likely have already achieved sub-percent accuracy in H_0.

Finally, we argue that the determination of M_{max} directly from the NS mass distribution is expected to be less prone to common systematic uncertainties. Mass measurement for BNS signals is driven by the low-order terms in the phase evolution which are well understood and modeled. Complementary methods of inferring the EoS and maximum mass simultaneously [24, 25, 65] rely on accurate tidal inference with improved waveform models than currently available and modeling of the EoS itself

to extrapolate from low to high densities. At the same time, methods based on information about the fate of the merger remnant are subject to systematics related to the interpretation of the post merger evolution and the electromagnetic emission [16, 18, 21]. In practice, we anticipate a multitude of methods utilizing different assumptions to be employed on future data; both a potential agreement and a potential disagreement between the different methods will teach us something about NSs and their properties.

Supplemental Material

POPULATION SIMULATION

The posterior distributions for the source parameters of observed GW signals are typically computed through stochastic sampling methods [72, 73]. For this study we consider hundreds of simulated BNS signals, which would make stochastic sampling from the full multidimensional posterior distribution computationally prohibitive. In this subsection, we instead describe how we estimate the measurement uncertainty for our simulated signals.

We draw parameters for each simulated system from a relevant astrophysical distribution. We assume that the SNR ρ is distributed according to ρ^{-4} [74], a reasonable assumptions for non-cosmological sources such as BNSs detected with detectors in current sensitivity. Though our analysis only considers the mass and not the spin distribution of BNSs, mass and spin measurements are correlated. We therefore simulate both in our population in order to achieve realistic mass measurement uncertainties. The effective spin χ_{eff} (see next section) is assumed to be uniformly distributed in $[-0.05, 0.05]$, while the mass distributions we consider ("Uniform", "UniformQ", and "Bimodal") are described in the main text.

Given the true parameters of the system, we approximate the likelihood for each parameter based on the following considerations. The main observable from BNS signals is the GW phase, whose evolution is determined by the system parameters. For long inspiral signals the phase can be expressed as a Taylor expansion around small velocities or, equivalently, large separations. This post-Newtonian (PN) expansion introduces terms at each order that depend on the system parameters. The first three terms in the expansion encode the component masses and spins with the PN coefficients Ψ_0, Ψ_2 and Ψ_3 corresponding to 0PN, 1PN, and 1.5PN orders respectively (a term of NPN order contains an extra factor of $(u/c)^{N/2}$ compared to the leading order term, where u is a characteristic velocity of the system, and c is the speed of light).

Given this, instead of assuming that the likelihood is gaussian in the parameters of interest (the component masses and spin) as is common, we assume that it is gaussian in Ψ_0, Ψ_2 and Ψ_3 with a standard deviation of σ_0, σ_2, and σ_3 respectively [33]. The values of the standard deviations are conservatively determined by comparison to the high-spin available results for GW170817 [42] and GW190425 [75]: $\sigma_0 = 0.0046\Psi_0/\rho$, $\sigma_2 = 0.2341\Psi_2/\rho$, and $\sigma_3 = -0.1293\Psi_3/\rho$, where we have also assumed that each measurement uncertainty is inversely proportional to the signal SNR.

For each binary with true parameters $(m_1, m_2, \chi_{\mathrm{eff}})$ and an SNR ρ we compute Ψ_0, Ψ_2, Ψ_3. We then draw $\Psi_{i,\mathrm{obs}}$ from $\mathcal{N}(\Psi_i, \sigma_i)$. The likelihood for each PN term Ψ_i is $\mathcal{N}(\Psi_{i,\mathrm{obs}}, \sigma_i)$, i.e. a normal distribution with a standard deviation of σ_i centered at the "observed" $\Psi_{i,\mathrm{obs}}$. We then sample independently from the likelihoods for the three PN coefficients and transform the result into samples for the likelihoods of $m_1, m_2, \chi_{\mathrm{eff}}$, taking into account the appropriate transformation Jacobian.

GRAVITATIONAL WAVE PHASE

In this subsection we collect the GW phase terms we use in order to simulate our BNS populations. Consider a compact binary with component masses m_1 and m_2 with $m_1 > m_2$ and dimensionless spins χ_1 and χ_2. In the following, we ignore the effect of spin-precession [76], as NS spins are expected to be small and there is no evidence for precession in the two detected BNS signals [4, 35]. This is a conservative assumption as spin-precession could potentially improve the measurement of the binary masses and spins [77, 78]. We define $\mathcal{M} = (m_1 m_2)^{3/5}/(m_1 + m_2)^{1/5}$, the chirp mass, $q = m_2/m_1$, the mass ratio, $\nu = q/(1 + q)^2$, the symmetric mass ra-

tio, $\delta m = (m_1 - m_2)/(m_1 + m_2)$, the mass difference, $\chi_{\text{eff}} = (m_1\chi_1 + m_2\chi_2)/(m_1 + m_2)$, the effective spin, and $\chi_a = (\chi_1 - \chi_2)/2$, the spin difference.

The phase of the frequency domain GW signal up to 1.5PN under the stationary phase approximation [79] is given by [80]

$$\Psi(f) = 2\pi f t_c - \phi_c - \frac{\pi}{4} \\ + \Psi_0(\mathcal{M})f^{-5/3} + \Psi_2(\mathcal{M},\nu)f^{-1} + \Psi_3(\mathcal{M},\nu,\beta)f^{-2/3}, \tag{3}$$

where t_c is the time of coalescence, ϕ_c is the phase of coalescence, and the three terms in the second line are the 0PN, 1PN, and 1.5PN terms respectively. The coefficient of each term is a function of the system intrinsic parameters with

$$\Psi_0(\mathcal{M}) = \frac{3}{128\mathcal{M}^{5/3}\pi^{5/3}}, \tag{4}$$

$$\Psi_2(\mathcal{M},\nu) = \frac{5}{96\mathcal{M}\pi\nu^{2/5}}\left(\frac{743}{336} + \frac{11\nu}{4}\right), \tag{5}$$

$$\Psi_3(\mathcal{M},\nu,\beta) = \frac{3\,(4\beta - 16\pi)}{128\mathcal{M}^{2/3}\pi^{2/3}\nu^{3/5}}, \tag{6}$$

where β is a linear function of the spins, encoding the leading-order spin-orbit coupling. The leading-order 0PN term, Ψ_0, is a function of the chirp mass only; being the largest contribution to the GW phase, this term is measured to exquisite precision for BNSs, which have typical $\mathcal{M}$ measurement errors of $\mathcal{O}(10^{-4})$ [34]. The 1PN term, Ψ_2, depends on the ratio of the binary component masses, and can be used in conjunction with $\mathcal{M}$ to measure the individual masses [81]. The 1.5PN coefficient, Ψ_3 contains two terms of different origin. The second term in the parenthesis, proportional to 16π, is a so-called tail-term [82], arising from scattering of the GWs off of the spacetime curvature as they propagate outwards from the binary near zone. The first term in the parenthesis, proportional to β, arises from the spin-orbit interaction between the binary components [83], given by

$$\beta = \frac{1}{3}\left(\frac{113 - 76\nu}{4}\chi_{\text{eff}} + \frac{76}{4}\delta m\nu\chi_a\right). \tag{7}$$

The simultaneous presence of β and ν in Ψ_3 results to the infamous spin-orbit degeneracy, deteriorating the measurement of both mass ratio and spins from GW signals [34]. Additionally, β represents the leading-order spin contribution, and it is thus the best measured spin parameter, akin to the chirp mass. It is common to disregard the second term in β and study directly the effective spin χ_{eff} for two reasons: (i) the second term is proportional to the mass difference and could be small, especially for BNS systems, and (ii) the effective spin χ_{eff} is conserved to at least 2PN order under spin-precession and radiation reaction [84]. We do the same for our simulations.

[1] F. Özel and P. Freire, Ann. Rev. Astron. Astrophys. **54**, 401 (2016), arXiv:1603.02698 [astro-ph.HE].

[2] J. M. Lattimer and M. Prakash, Phys. Rept. **621**, 127 (2016), arXiv:1512.07820 [astro-ph.SR].

[3] B. P. Abbott et al. (LIGO Scientific Collaboration, Virgo Collaboration), Phys. Rev. Lett. **119**, 161101 (2017), arXiv:1710.05832 [gr-qc].

[4] B. P. Abbott et al. (LIGO Scientific, Virgo), (2020), arXiv:2001.01761 [astro-ph.HE].

[5] J. Aasi et al. (LIGO Scientific Collaboration), Class. Quant. Grav. **32**, 074001 (2015), arXiv:1411.4547 [gr-qc].

[6] F. Acernese et al. (Virgo Collaboration), Class. Quant. Grav. **32**, 024001 (2015), arXiv:1408.3978 [gr-qc].

[7] É. É. Flanagan and T. Hinderer, Phys. Rev. D **77**, 021502 (2008), arXiv:0709.1915 [astro-ph].

[8] J.-P. Lasota, P. Haensel, and M. A. Abramowicz, Astrophys. J. **456**, 300 (1996), arXiv:astro-ph/9508118 [astro-ph].

[9] J. Antoniadis, P. C. Freire, N. Wex, T. M. Tauris, R. S. Lynch, et al., Science **340**, 6131 (2013), arXiv:1304.6875 [astro-ph.HE].

[10] H. T. Cromartie et al., Nature Astronomy , 1 (2019), arXiv:1904.06759 [astro-ph.HE].

[11] S. Han and A. W. Steiner, Phys. Rev. D **99**, 083014 (2019), arXiv:1810.10967 [nucl-th].

[12] J. Antoniadis, T. M. Tauris, F. Ozel, E. Barr, D. J. Champion, and P. C. C. Freire, (2016), arXiv:1605.01665 [astro-ph.HE].

[13] J. Alsing, H. O. Silva, and E. Berti, Mon. Not. Roy. Astron. Soc. **478**, 1377 (2018), arXiv:1709.07889 [astro-ph.HE].

[14] S. Lawrence, J. G. Tervala, P. F. Bedaque, and M. Miller, Astrophys. J. **808**, 186 (2015), arXiv:1505.00231 [astro-ph.HE].

[15] A. Bauswein, T. W. Baumgarte, and H.-T. Janka, Phys. Rev. Lett. **111**, 131101 (2013).

[16] B. Margalit and B. D. Metzger, Astrophys. J. **880**, L15 (2019), arXiv:1904.11995 [astro-ph.HE].

[17] A. Bauswein, S. Blacker, V. Vijayan, N. Stergioulas, K. Chatziioannou, J. A. Clark, N.-U. F. Bastian, D. B. Blaschke, M. Cierniak, and T. Fischer, (2020), arXiv:2004.00846 [astro-ph.HE].

[18] B. Margalit and B. D. Metzger, Astrophys. J. **850**, L19 (2017), arXiv:1710.05938 [astro-ph.HE].

[19] M. Ruiz, S. L. Shapiro, and A. Tsokaros, Phys. Rev. D**97**, 021501 (2018), arXiv:1711.00473 [astro-ph.HE].

[20] M. Shibata, S. Fujibayashi, K. Hotokezaka, K. Kiuchi, K. Kyutoku, Y. Sekiguchi, and M. Tanaka, Phys. Rev. D**96**, 123012 (2017), arXiv:1710.07579 [astro-ph.HE].

[21] L. Rezzolla, E. R. Most, and L. R. Weih, Astrophys. J. **852**, L25 (2018), arXiv:1711.00314 [astro-ph.HE].

[22] M. Shibata, E. Zhou, K. Kiuchi, and S. Fujibayashi, Phys. Rev. D**100**, 023015 (2019), arXiv:1905.03656 [astro-ph.HE].

[23] B. P. Abbott et al. (LIGO Scientific, Virgo), Class. Quant. Grav. **37**, 045006 (2020), arXiv:1908.01012 [gr-qc].

[24] P. Landry and R. Essick, Phys. Rev. D **99**, 084049 (2019), arXiv:1811.12529 [gr-qc].

[25] R. Essick, P. Landry, and D. E. Holz, Phys. Rev. D**101**, 063007 (2020), arXiv:1910.09740 [astro-ph.HE].

[26] W. M. Farr, N. Sravan, A. Cantrell, L. Kreidberg, C. D. Bailyn, I. Mandel, and V. Kalogera, Astrophys. J. **741**, 103 (2011), arXiv:1011.1459 [astro-ph.GA].

[27] L. Kreidberg, C. D. Bailyn, W. M. Farr, and V. Kalogera, The Astrophysical Journal **757**, 36 (2012).

[28] T. A. Thompson *et al.*, (2018), 10.1126/science.aau4005, arXiv:1806.02751 [astro-ph.HE].

[29] B. P. Abbott *et al.* (LIGO Scientific Collaboration, Virgo Collaboration), Living Rev. Rel. **19**, 1 (2013), arXiv:1304.0670 [gr-qc].

[30] T. M. Tauris *et al.*, Astrophys. J. **846**, 170 (2017), arXiv:1706.09438 [astro-ph.HE].

[31] M. Dominik, K. Belczynski, C. Fryer, D. E. Holz, E. Berti, T. Bulik, I. Mandel, and R. O'Shaughnessy, The Astrophysical Journal **759**, 52 (2012).

[32] N. Farrow, X.-J. Zhu, and E. Thrane, Astrophys. J. **876**, 18 (2019), arXiv:1902.03300 [astro-ph.HE].

[33] K. K. Y. Ng, S. Vitale, A. Zimmerman, K. Chatziioannou, D. Gerosa, and C.-J. Haster, Phys. Rev. **D98**, 083007 (2018), arXiv:1805.03046 [gr-qc].

[34] C. Cutler and E. E. Flanagan, Phys. Rev. D **49**, 2658 (1994).

[35] B. P. Abbott *et al.* (LIGO Scientific, Virgo), Phys. Rev. X **9**, 011001 (2019), arXiv:1805.11579 [gr-qc].

[36] I. Mandel, Phys. Rev. D **81**, 084029 (2010), arXiv:0912.5531 [astro-ph.HE].

[37] D. W. Hogg, A. D. Myers, and J. Bovy, The Astrophysical Journal **725**, 2166 (2010).

[38] T. J. Loredo, in *American Institute of Physics Conference Series*, American Institute of Physics Conference Series, Vol. 735, edited by R. Fischer, R. Preuss, and U. V. Toussaint (2004) pp. 195–206, arXiv:astro-ph/0409387 [astro-ph].

[39] I. Mandel, W. M. Farr, and J. R. Gair, Mon. Not. Roy. Astron. Soc. **486**, 1086 (2019), arXiv:1809.02063 [physics.data-an].

[40] The LIGO Scientific Collaboration and the Virgo Collaboration, arXiv e-prints , arXiv:1811.12907 (2018), arXiv:1811.12907 [astro-ph.HE].

[41] B. P. Abbott *et al.* (LIGO Scientific, Virgo), Phys. Rev. Lett. **121**, 161101 (2018), arXiv:1805.11581 [gr-qc].

[42] L. S. Collaboration, https://dcc.ligo.org/LIGO-P1800061/public (2018).

[43] M. F. Carney, L. E. Wade, and B. S. Irwin, Phys. Rev. D **98**, 063004 (2018), arXiv:1805.11217 [gr-qc].

[44] M. C. Miller, C. Chirenti, and F. K. Lamb, (2019), 10.3847/1538-4357/ab4ef9, arXiv:1904.08907 [astro-ph.HE].

[45] P. Landry, R. Essick, and K. Chatziioannou, (2020), arXiv:2003.04880 [astro-ph.HE].

[46] T. Hinderer, Astrophys.J. **677**, 1216 (2008), arXiv:0711.2420 [astro-ph].

[47] T. Hinderer, B. D. Lackey, R. N. Lang, and J. S. Read, Phys. Rev. D **81**, 123016 (2010), arXiv:0911.3535 [astro-ph.HE].

[48] A. Torres-Rivas, K. Chatziioannou, A. Bauswein, and J. A. Clark, Phys. Rev. D **99**, 044014 (2019), arXiv:1811.08931 [gr-qc].

[49] G. Montana, L. Tolos, M. Hanauske, and L. Rezzolla, Phys. Rev. D **99**, 103009 (2019), arXiv:1811.10929 [astro-ph.HE].

[50] K. Chatziioannou and S. Han, Phys. Rev. **D101**, 044019 (2020), arXiv:1911.07091 [gr-qc].

[51] T. M. Tauris and H.-T. Janka, Astrophys. J. **886**, L20 (2019), arXiv:1909.12318 [astro-ph.SR].

[52] R. Magee, A.-S. Deutsch, P. McClincy, C. Hanna, C. Horst, D. Meacher, C. Messick, S. Shandera, and M. Wade, Phys. Rev. **D98**, 103024 (2018), arXiv:1808.04772 [astro-ph.IM].

[53] B. P. Abbott *et al.* (LIGO Scientific, Virgo), Phys. Rev. Lett. **121**, 231103 (2018), arXiv:1808.04771 [astro-ph.CO].

[54] B. P. Abbott *et al.* (LIGO Scientific, Virgo), Phys. Rev. Lett. **123**, 161102 (2019), arXiv:1904.08976 [astro-ph.CO].

[55] H.-Y. Chen and K. Chatziioannou, (2019), arXiv:1903.11197 [astro-ph.HE].

[56] C. Barbieri, O. S. Salafia, M. Colpi, G. Ghirlanda, and A. Perego, (2020), arXiv:2002.09395 [astro-ph.HE].

[57] A. Chen, N. K. Johnson-McDaniel, T. Dietrich, and R. Dudi, (2020), arXiv:2001.11470 [astro-ph.HE].

[58] S. R. Taylor, J. R. Gair, and I. Mandel, Phys. Rev. D **85**, 023535 (2012), arXiv:1108.5161 [gr-qc].

[59] W. M. Farr, M. Fishbach, J. Ye, and D. Holz, Astrophys. J. **883**, L42 (2019), arXiv:1908.09084 [astro-ph.CO].

[60] B. Farr *et al.*, Astrophys. J. **825**, 116 (2016), arXiv:1508.05336 [astro-ph.HE].

[61] H.-Y. Chen, M. Fishbach, and D. E. Holz, Nature **562**, 545 (2018), arXiv:1712.06531 [astro-ph.CO].

[62] S. Hild *et al.*, Classical and Quantum Gravity **28**, 094013 (2011), arXiv:1012.0908 [gr-qc].

[63] D. Reitze *et al.*, Bull. Am. Astron. Soc. **51**, 035 (2019), arXiv:1907.04833 [astro-ph.IM].

[64] S. R. Taylor and J. R. Gair, Phys. Rev. D **86**, 023502 (2012), arXiv:1204.6739 [astro-ph.CO].

[65] D. Wysocki, R. O'Shaughnessy, L. Wade, and J. Lange, (2020), arXiv:2001.01747 [gr-qc].

[66] J. D. Hunter, Computing In Science & Engineering **9**, 90 (2007).

[67] B. Carpenter, A. Gelman, M. Hoffman, D. Lee, B. Goodrich, M. Betancourt, M. Brubaker, J. Guo, P. Li, and A. Riddell, Journal of Statistical Software, Articles **76**, 1 (2017).

[68] T. Oliphant, "NumPy: A guide to NumPy," USA: Trelgol Publishing (2006), [Online].

[69] P. Virtanen *et al.*, Nature Methods **17**, 261 (2020).

[70] Astropy Collaboration, Astronomy and Astrophysics **558**, A33 (2013), arXiv:1307.6212 [astro-ph.IM].

[71] A. M. Price-Whelan *et al.*, American Astronomical Society **156**, 123 (2018).

[72] J. Veitch *et al.*, Phys. Rev. D **91**, 042003 (2015), arXiv:1409.7215 [gr-qc].

[73] B. P. Abbott *et al.* (LIGO Scientific, Virgo), Phys. Rev. Lett. **116**, 241102 (2016), arXiv:1602.03840 [gr-qc].

[74] H.-Y. Chen and D. E. Holz, arXiv e-prints (2014), arXiv:1409.0522 [gr-qc].

[75] L. S. Collaboration, https://dcc.ligo.org/LIGO-P2000026/public (2020).

[76] T. A. Apostolatos, C. Cutler, G. J. Sussman, and K. S. Thorne, Phys.Rev. **D49**, 6274 (1994).

[77] M. Hannam, D. A. Brown, S. Fairhurst, C. L. Fryer, and I. W. Harry, Astrophys. J. **766**, L14 (2013), arXiv:1301.5616 [gr-qc].

[78] K. Chatziioannou, N. Cornish, A. Klein, and N. Yunes, Astrophys. J. **798**, L17 (2015), arXiv:1402.3581 [gr-qc].

[79] S. Droz, D. J. Knapp, E. Poisson, and B. J. Owen, Phys.Rev. **D59**, 124016 (1999), arXiv:gr-qc/9901076 [gr-qc].

[80] L. Blanchet, Living Rev. Rel. **17**, 2 (2014), arXiv:1310.1528 [gr-qc].

[81] R. V. Wagoner and C. M. Will, Astrophys. J. **210**, 764 (1976).

[82] E. Poisson, Phys. Rev. D **47**, 1497 (1993).

[83] L. E. Kidder, C. M. Will, and A. G. Wiseman, Phys. Rev. D **47**, R4183 (1993).

[84] E. Racine, Phys.Rev. **D78**, 044021 (2008), arXiv:0803.1820 [gr-qc].